CHAPTER IV

EFFECTS OF OXIDE SUPPORTS ON ETHYLENE EPOXIDATION ACTIVITY OVER Ag-BASED CATALYSTS

(Published in Journal of Molecular Catalysis A: Chemical, 358, 2012, 58-66)

4.1 Abstract

In this study, Ag-based catalysts with different loadings on various oxide supports, including low-surface-area α-Al_2O_3, Al_2O_3 C, $Al_2O_{3,Acid}$, SiO_2 90, TiO_2 and $SrTiO_3$ synthesized by a sol-gel process, were investigated for ethylene epoxidation over a range of reaction temperatures. The specific surface area, crystallinity, surface morphology, oxidation state, metal crystallite size, and oxygen and ethylene adsorption characteristics of all prepared catalysts were characterized and correlated to the ethylene epoxidation activity. Compared with conventional Ag catalysts supported on low-surface-area α-Al_2O_3, the 17.16 wt.% Ag/$SrTiO_3$ catalyst exhibited much better catalytic activity for the ethylene epoxidation reaction, providing both the highest EO yield of 4.5 % and EO selectivity up to 99 %. The results indicate that high oxygen and ethylene uptakes, together with the large size of Ag particles, play an important role in achieving the best catalytic activity of the Ag/$SrTiO_3$ catalyst towards ethylene epoxidation reaction.

Keywords: Ethylene epoxidation; $SrTiO_3$; Sol-gel; α-Alumina; Ag

4.2 Introduction

The epoxidation of ethylene to ethylene oxide (EO) over Ag catalysts is an important industrial process since EO is one of the highest volume petrochemicals, accounting for approximately 40-50 % of the total value of organic chemicals with 86 % of the global capacity utilization [1-2]. Moreover, the world consumption of EO in 2009 was 19 million metric tons per year, making it the most utilized epoxide species [3]. It is mainly used to produce ethylene glycol (EG) and surface-active agents. Several dozen important fine chemical intermediates are derivatives of EO. In addition, it is extensively used in other various applications, such as washing/dying, electronics, pharmaceuticals, pesticides, textiles, papermaking, and automobile parts.

The most widely used process for EO production is the direct catalytic oxidation of ethylene with air or oxygen over Ag-based catalysts [4]. According to the high selectivity towards ethylene epoxidation, as well as their inertness for the isomerization of EO to acetaldehyde, the industrial catalyst supports of α-Al_2O_3, especially low surface area α-Al_2O_3 (specific surface area < 1 m^2/g), with high Ag loadings are widely used [5]. However, these catalysts possess relatively low yields of EO as a result of poorly dispersed Ag particles on these commercial Al_2O_3 supports [6]. Therefore, there is a motivation to develop new catalysts with alternative supports to offer higher catalytic performance of ethylene epoxidation. In industrial practice, a typical per pass ethylene conversions is 20-30 % with 79-80 % selectivity. The reaction temperature is usually controlled in the range of 493-548 K, with pressures in the range of 1-3 MPa (10-30 atmospheres) [4].

There were a number of studies about the effect of supports on epoxidation of ethylene. Rojluechai et al. [7-8] reported in a catalytic activity study of Au, Ag, and Au–Ag catalysts on Al_2O_3, TiO_2, and CeO_2 that the support played an important role in the ethylene epoxidation reaction. The best performance for ethylene epoxidation was found to occur over Ag catalysts supported on Al_2O_3 with the optimum Ag loading of 13.18 wt.%, while on Ag catalysts supported on TiO_2 or CeO_2 only total oxidation was observed.

Apart from Al_2O_3, Ag catalysts supported on relatively high surface area SiO_2 (specific surface area up to ca. 350 m^2/g) were also reported to be active for EO

production, giving in some cases EO selectivity similar to that obtained with low surface area α-Al_2O_3 [9]. Beck et al. [10] developed mesoporous silicates to reduce the mass diffusion limitations and to provide the acidic properties of the microporous zeolitic aluminosilicates, which directly affected the catalytic activity. The very high surface area and narrow pore size distributions of these supports allowed uniform dispersion of metal active sites even at high metal loadings, without inducing any negative effects on catalytic reaction rates due to diffusion limitations.

Fotopoulos and Triantafyllidis [11] compared the ethylene epoxidation activity of Ag catalysts supported on non-porous SiO_2, microporous silicalite zeolite, and MCM-41 and HMS mesoporous silicates to conventional low surface area α-Al_2O_3. They found that the Ag catalysts supported on MCM-41 and HMS mesoporous silicates were active in ethylene epoxidation reaction, exhibiting EO selectivity similar to or slightly lower than those of the Ag catalysts supported on non-porous SiO_2 and conventional low surface area α-Al_2O_3 at a relatively low temperature (~503 K). Among the two types of mesoporous silicates, the HMS with wormhole-like structure was a more appropriate support for moderate Ag loadings (up to ca. 20 wt.%). The main benefit of using HMS and MCM-41 mesoporous materials is their ability to support very high Ag loadings (ca. 40 wt.%) without increasing Ag crystallite size to more than ca. 20 nm. As a consequence, the highly loaded mesoporous-based catalysts showed very high ethylene conversion (up to 65 %) at a relatively low temperature (~493 K), with acceptable EO selectivity (~30–35 %). So far, there have been some attempts to develop new mesoporous supports with uniform porous structures to improve the activity towards specific reactions. Particularly, Puangpetch et al. [12] successfully synthesized mesoporous-assembled $SrTiO_3$ nanocrystals via a sol-gel process with the aid of a structure-directing surfactant. These mesoporous-assembled structures with a high pore uniformity of $SrTiO_3$ proved to be active for photocatalytic water splitting. One of the objectives of this work was to explore the use of this mesoporous-structured $SrTiO_3$ as the support for Ag, as it was hypothesized to facilitate the formation of uniform nanosized Ag particles at high Ag loadings which can, in turn, facilitate the epoxidation reaction.

Furthermore, some researchers tried to modify conventional supports [13-14] or to study some specific process parameters to enhance the EO selectivity [15].

Serafin [16] reviewed the silver-catalyzed epoxidation of ethylene from both a surface-science as well as industrial perspective, and discussed the roles of promoters and moderators. Hassani et al. [17] compared different impregnation techniques on α-Al_2O_3 support to make catalysts with high Ag contents and dispersion using silver nitrate and silver oxide together with oxalic and lactic acids. They claimed that the catalysts prepared by their method provided much higher Ag dispersion than commercial catalysts. Moreover, Christopher and Linic [18] concluded that the selectivity for ethylene oxide was governed by the nature of the Ag surface facets, the abundance of unselective under-coordinated surface sites, and the operating conditions. They showed experimentally that the reaction selectivity could be manipulated by controlling the shape and size of Ag particles. The Ag nanocubes exhibited higher selectivity than either Ag nanowires or nanospheres. For a given shape, larger particles offered a higher EO selectivity. From all of the previous studies, it can be concluded that the nature of the support and Ag particle size significantly affect the ethylene epoxidation activity and selectivity.

In this work, the effects of various oxide supports for Ag catalysts on EO selectivity and yield were investigated. The catalytic performance was correlated with the physical properties of the prepared catalysts, including specific surface area, crystallinity, Ag particle size, surface morphology, oxidation state, and oxygen and ethylene adsorption characteristics. The Ag catalyst supported on α-Al_2O_3 was used as a benchmark catalyst for catalytic activity in comparisons with Ag catalysts on various oxide supports under atmospheric pressure, leading to low conversions of both ethylene and oxygen as compared to most industrial reactors operated at a very high pressure with recycling to yield much higher conversions, as mentioned before. However, both EO selectivity and yield could be used to compare the catalytic activities of all synthesized Ag catalysts on different oxide supports.

4.3 Experimental

4.3.1 Materials

Aluminium oxide C (Al_2O_3, 85-115 m^2/g) and hydrophilic fumed silica 90 (SiO_2, 75-105 m^2/g) were obtained from Degussa AG. α-Al_2O_3 (0.109 m^2/g)

was supplied by Fluka. $Al_2O_{3,Acid}$ was supplied by Aldrich. Silver nitrate ($AgNO_3$) was supplied by S.R. Lab. Tetraisopropyl orthotitanate (TIPT, $Ti(OCH(CH_3)_2)_4$), strontium nitrate ($Sr(NO_3)_2$), and laurylamine (LA, $CH_3(CH_2)_{11}NH_2$) were purchased from Merck. Acetylacetone (ACA, $CH_3COCH_2COCH_3$) was obtained from S.D. Fine-Chemical. Analytical grade Hydrochloric acid (HCl) and ethanol (C_2H_5OH) were purchased from Labscan. All chemicals were used without further purification.

4.3.2 Catalyst preparation procedures

In this work, all supported Ag catalysts were prepared by the incipient wetness impregnation. Various aluminium oxides (Al_2O_3 C, α-Al_2O_3, and $Al_2O_{3,Acid}$) were impregnated with an aqueous silver nitrate solution to achieve nominal Ag loadings of 10, 13.5, 15, and 20 wt.%. After the impregnation step, the catalysts were dried at 383 K overnight, followed by calcination in air at 773 K for 5 h. Apart from the synthesis of Ag catalysts on various Al_2O_3 materials, Ag catalysts on SiO_2 90 and mesoporous-assembled $SrTiO_3$ were also prepared to achieve various nominal Ag loadings by the same procedure.

The mesoporous-assembled $SrTiO_3$ support was synthesized by a sol-gel process with the aid of a structure-directing surfactant [12,19-22]. Firstly, the TIPT and ACA with a molar ratio of 1:1 were mixed together. The mixed TIPT/ACA solution was gently shaken until homogeneous mixing was achieved. A required amount of $Sr(NO_3)_2$, based on the Sr-to-Ti molar ratio of 1:1, was dissolved in 24 ml of distilled water in a separate beaker. Next, 36 ml of ethanol was mixed with the as-prepared $Sr(NO_3)_2$ solution. After that, 1.112 g of the LA and 0.5 ml of HCl were added to obtain the $Sr(NO_3)_2$/LA/HCl solution. The $Sr(NO_3)_2$/LA/HCl solution was poured into the TIPT/ACA solution. The final mixture was continuously stirred at room temperature until a homogeneous transparent sol was obtained. Then, the sol-containing solution was placed in an oven at 353 K for 4 d for complete gelation. Afterwards, the gel was dried at 353 K for 4 d to eliminate the solvents. Finally, the dried gel was calcined at 773 K to produce the desired mesoporous-assembled $SrTiO_3$ support. The synthesized $SrTiO_3$ support was then impregnated to obtain various Ag loadings by the incipient wetness impregnation procedure explained above.

In addition, a nanocrystalline mesoporous TiO_2 support was synthesized via a sol-gel process with surfactant-assisted template in a TIPT/LAHC modified with ACA system similar to the mesoporous-assembled $SrTiO_3$ support [21], followed by impregnating step to obtain various Ag loadings. The prepared Ag loaded TiO_2 catalysts were also tested for their catalytic activity towards the ethylene epoxidation in order to compare with the other studied catalysts.

4.3.3 Catalyst characterization techniques

All synthesized catalyst samples were characterized to determine the specific surface area via N_2 adsorption at 77 K by using a surface area analyzer (Quantachrome, SAA-1MP). Prior to the analysis, each catalyst sample was outgassed at 473 K for 8 h. The actual contents of Ag loaded on the catalyst samples were analyzed by an atomic adsorption spectrophotometer (AAS, Varian, Spectr AA-300).

The crystalline structures of the catalysts were examined by an X-ray diffractometer (XRD, Rigaku, RINT 2200 HV) equipped with a Ni filter and a Cu Kα radiation source (λ = 1.542 Å) operating at 40 kV and 30 mA. The catalyst samples were scanned in the range of 2θ from 5° to 90° in a continuous mode with the scanning rate of 5° min^{-1}. The Ag crystallite size (D) was calculated from X-ray line broadening of the Ag crystalline peak using the Debye-Scherrer equation [23,24] with the full line width at half maximum of intensity and the 2θ value, as follows:

$$D = \frac{0.9\lambda}{B\cos\theta}$$

where λ is the x-ray wavelength (1.542 Å for Cu source), B is the line broadening, and θ is the Bragg angle. The dispersion and surface area of the Ag particles were determined using a H_2 chemisorption apparatus (Micromeritics, ASAP 2020). The catalyst samples were reduced at 873 K in 5 % H_2 in N_2 atmosphere before the analysis.

The surface morphology of some selected catalysts was observed by a field emission scanning electron microscope (FE-SEM, JEOL 5200-2AE). The samples were coated with Pt to improve their conductivity before the examination. The catalyst morphology was also observed by transmission electron microscopy

(TEM, JEOL 3011 at 300 kV and JEOL 2010 at 200 kV). The specimens for the TEM analysis were prepared by ultrasonically dispersing powders of the catalysts in ethanol and then placing drops of the suspension onto a Cu grid coated with a carbon film. The existence of Ag particles on different supports was verified by using an energy dispersive X-ray spectroscope (EDS) attached to the TEM. The Ag particle sizes were determined from statistical analysis of the diameters of particles visible in the TEM images.

The oxidation state of the supported Ag particles was analyzed by an X-ray photoelectron spectroscope (XPS, Shimadzu, Kratos). A monochromatic Al Kα source was used as the X-ray source. The relative surface charging of the samples was corrected by referencing all the energies to the C1s level as an internal standard at 285 eV [25]. Coke formation on the spent catalysts was analyzed by a thermogravimetric-differential thermal analyzer (TG-DTA, PerkinElmer, Pyris Diamond).

Temperature-programmed desorption (TPD) experiments were carried out using a TPD analyzer (Quantachrome, Chembet 3000). The instrument was connected to a thermal conductivity detector (TCD). High-purity He was used as the carrier gas with a flow rate of 20 cm^3/min. The catalyst powders were placed into a quartz tube reactor, which was heated by a furnace. For the TPD experiments of both oxygen and ethylene, the catalysts were initially heated at 473 K for 30 min under high-purity He atmosphere in order to remove moisture and impurities from their surface. Then, oxygen (4.99 % O_2 in He) or pure ethylene (99.99 % C_2H_4) was allowed to adsorb onto the catalyst surface at 473 K for 2 h. After that, the catalyst samples were cooled to room temperature in a stream of high-purity He. The catalyst samples were then heated from room temperature to 1173 K with a heating rate of 10 K/min, and the desorbed gas was swept by high-purity He. The concentration profile of either oxygen or ethylene present in the effluent stream was measured by the TCD.

4.3.4 Activity testing experiments

The epoxidation reaction of ethylene was conducted in a packed-bed 8-mm ID tubular reactor, which was operated at 24.7 psia. 30 mg catalyst powder was placed inside a quartz tube reactor and secured by two layers of glass wool. The reactor was placed in the furnace equipped with a temperature controller. The catalyst was pretreated with oxygen at 473 K for 2 h. The feed gas was a mixture of 40 % ethylene in He, pure oxygen (HP grade), and pure helium (HP grade). Feed gas compositions of 6 % ethylene and 6 % oxygen with helium balance were achieved by using mass flow controllers. The space velocity through the reactor was maintained at 6,000 h^{-1}, and the reaction temperature was varied from 473 to 573 K. The compositions of the feed and product gases were analyzed by using an on-line gas chromatograph (Perkin Elmer, ARNEL) equipped with a 60/80 CARBOXEN 1 packed column (capable of separating carbon dioxide, ethylene, and oxygen) and a Rt-U PLOT capillary column (capable of separating EO, ethane, and propane). It should be noted that the formation of acetaldehyde was not quantified. It appeared only in trace amounts since under the studied conditions acetaldehyde underwent further oxidation to carbon dioxide and water [7]. The catalytic activity of each studied catalyst was evaluated at 6 h in which the system reached steady state condition. The experimental data with less than 5 % error were averaged to assess the catalytic performance. Moreover, for the best $Ag/SrTiO_3$ catalyst, the system was operated up to 48 h to observe the long-term stability of the catalyst.

4.4 Results and Discussion

4.4.1 Catalyst characterization results

4.4.1.1 Specific surface area results

Table 4.1 shows the specific surface areas of the catalysts prepared with different oxide supports at their optimum Ag loadings (based on the catalytic activity results in terms of EO selectivity and yield). Among the studied catalysts, the α-Al_2O_3-supported catalyst possessed the lowest specific surface area, followed by the $SrTiO_3$-supported catalyst, while the $Al_2O_{3,Acid}$-supported catalyst had the highest specific surface area. For each of the supports, the specific surface

area decreased slightly with increasing Ag loading (data not shown here), implying that this catalyst preparation technique can provide well-dispersed Ag particles on the support surface [8].

4.4.1.2 Metal dispersion results

The dispersion, specific surface area, particle size and crystallite size of Ag particles on different oxide supports are also shown in Table 4.1. It can be seen that the Ag dispersion is directly proportional to the Ag specific surface area. In comparisons among the studied catalysts, the 14.71 wt.% Ag/SiO_2 90 had the highest Ag dispersion while the lowest Ag dispersion was observed for the Ag/α-Al_2O_3 and $Ag/SrTiO_3$ catalysts.

4.4.1.3 Surface morphology

As will be shown later, the $Ag/SrTiO_3$ catalysts exhibited the highest catalytic activity in terms of EO selectivity and yield. Therefore, the present work focused to investigate the surface morphology of the $Ag/SrTiO_3$ catalysts. Figure 4.1 displays the SEM images of the $Ag/SrTiO_3$ catalysts with different Ag loadings. The Ag loading altered the textural properties of the $Ag/SrTiO_3$ catalysts. The surface topology of the $Ag/SrTiO_3$ catalysts changed as the Ag loading was increased, and large aggregates of Ag particles were formed at about 17 wt.% Ag or higher.

Table 4.1 Characteristics of Ag catalysts on different supports at optimum Ag loadings

Support	Ag loading	Specific surface area	Ag dispersion[a]	Ag specific surface area[a]		Ag particle size[b]	Ag crystallite size[c]
	(wt.%)	(m^2/g)	(%)	m^2/g_{sample}	m^2/g_{metal}	(nm)	(nm)
α-Al_2O_3	14.86	0.03 (0.1)*	0.03	0.02	0.15	43.6 ± 0.4	49.8
Al_2O_3 C	13.16	89.8 (98.3)*	0.06	0.04	0.31	27.7 ± 0.5	30.6
$Al_2O_{3,Acid}$	14.90	108.5 (123.0)*	0.08	0.06	0.37	25.1 ± 0.5	27.9
SiO_2 90	14.71	58.8 (86.9)*	0.19	0.14	0.90	42.1 ± 0.4	41.5
$SrTiO_3$	17.16	3.0 (4.4)*	0.03	0.03	0.16	58.6 ± 0.4	52.1
TiO_2	14.67	28.6 (36.7)*	-	-	-	44.4 ± 0.5	43.2

[a] From H_2 chemisorption analysis
[b] From TEM analysis
[c] From XRD analysis
* Specific surface area of support without Ag loading

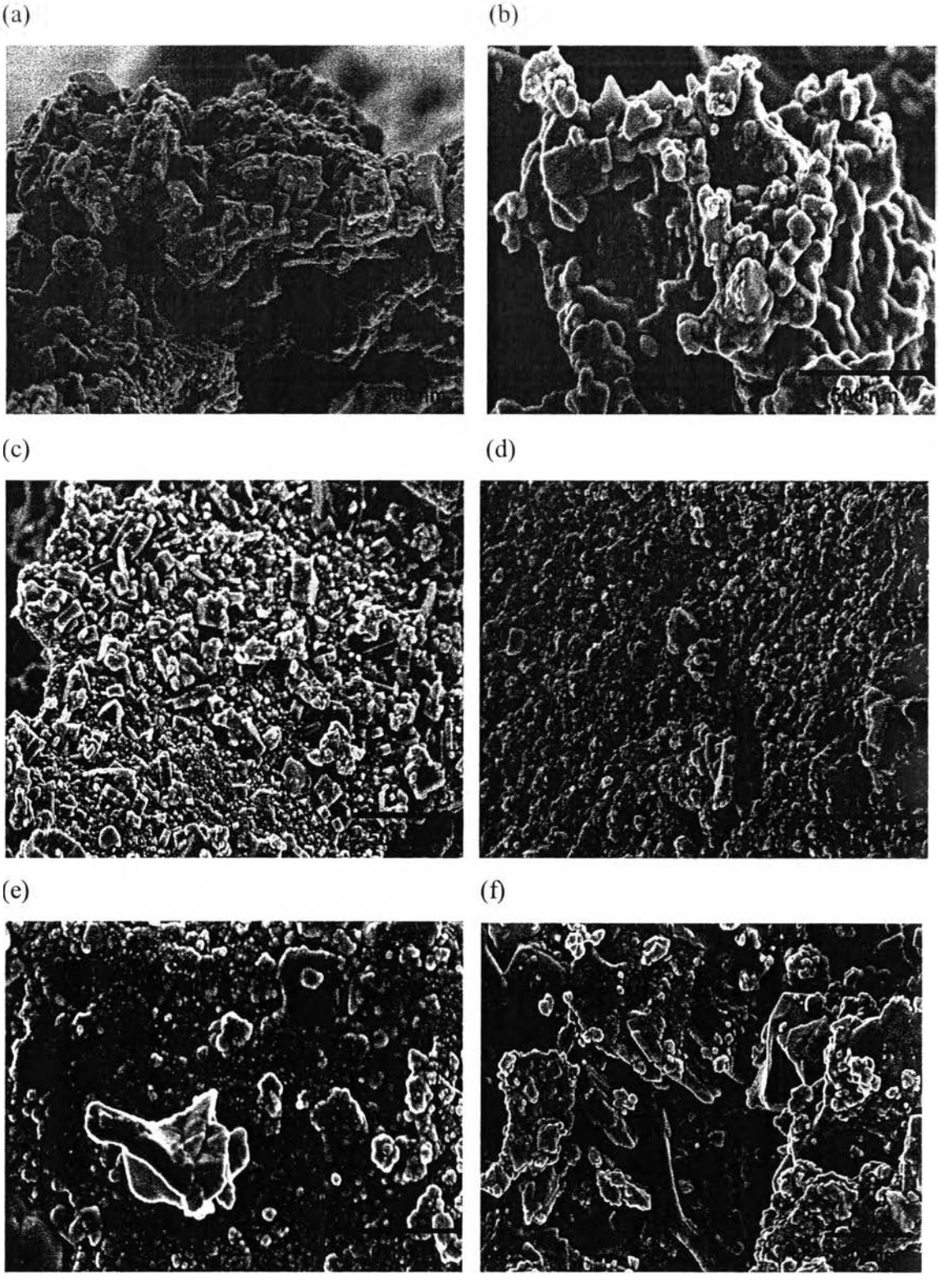

Figure 4.1 SEM images of $SrTiO_3$ catalysts without Ag loading (a) and with Ag loadings of 12.38 wt.% (b), 13.41 wt.% (c), 14.85 wt.% (d), 17.16 wt.% (e), and 19.74 wt.% (f).

The TEM/EDS technique was used to verify the existence of Ag nanoparticles on the studied $SrTiO_3$ support. The TEM images of the 17.16 wt.% $Ag/SrTiO_3$ catalyst are shown in Figures 4.2a and 4.2b, while Figure 4.2c reveals the selected area diffraction (SAD) pattern of this catalyst, which confirms the single crystalline structure of the $Ag/SrTiO_3$ catalyst. The Ag(110) plane can also be clearly seen in Figure 4.2d, indicating the highly crystalline structure of Ag nanoparticles. Figures 4.3a and 4.3b exemplify the TEM images of the 13.16 wt.% Ag/Al_2O_3 C and the 14.86 wt.% Ag/α-Al_2O_3, indicating the inhomogeneous dispersion of Ag nanoparticles throughout the two different Al_2O_3 supports (Al_2O_3 C and α-Al_2O_3). The average sizes of Ag nanoparticles in all the studied catalysts are summarized in Table 4.1. For any given support, the sizes of Ag particle and crystalline suggest that this catalyst preparation technique can provide single crystals of Ag deposition on all studied supports. Among the studied supports, the largest average Ag particle size (59 nm) was found on the $SrTiO_3$ support, while the smallest average Ag particle size (25 nm) was found on the $Al_2O_{3,Acid}$ support. The Ag particle size of $Ag/SrTiO_3$ catalysts increased from 47 nm (12.38 wt.% Ag), to 48 nm (13.41 wt.% Ag), and 50 nm (14.85 wt.% Ag), 59 nm (17.16 wt.% Ag) and 66 nm (19.74 wt.% Ag). The results are consistent with large aggregates of Ag particles at 17 wt.% Ag or higher as shown in the SEM images.

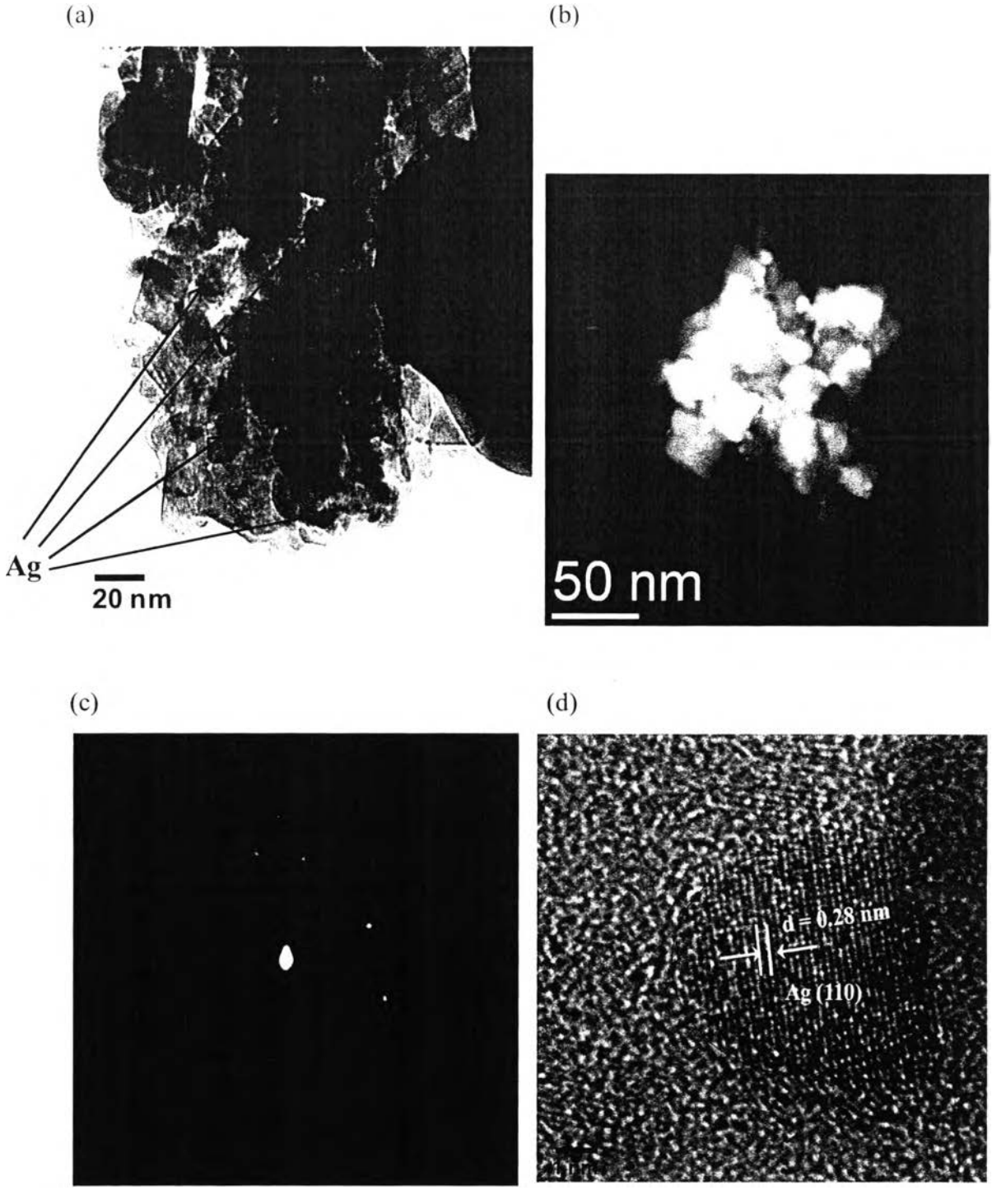

Figure 4.2 TEM images of 17.16 wt.% Ag/$SrTiO_3$ catalyst: (a) bright-field image, (b) z-contrast image, (c) SAD pattern, and (d) Ag(110) plane.

(a)

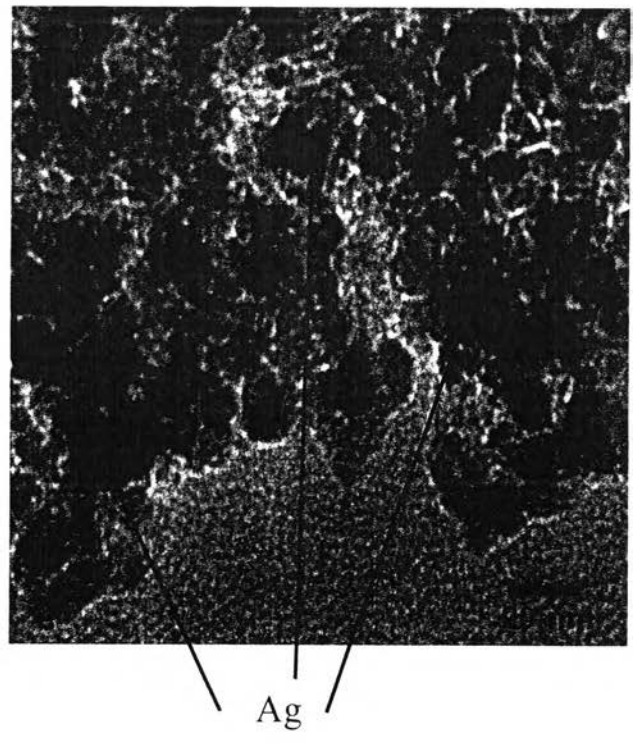

(b)

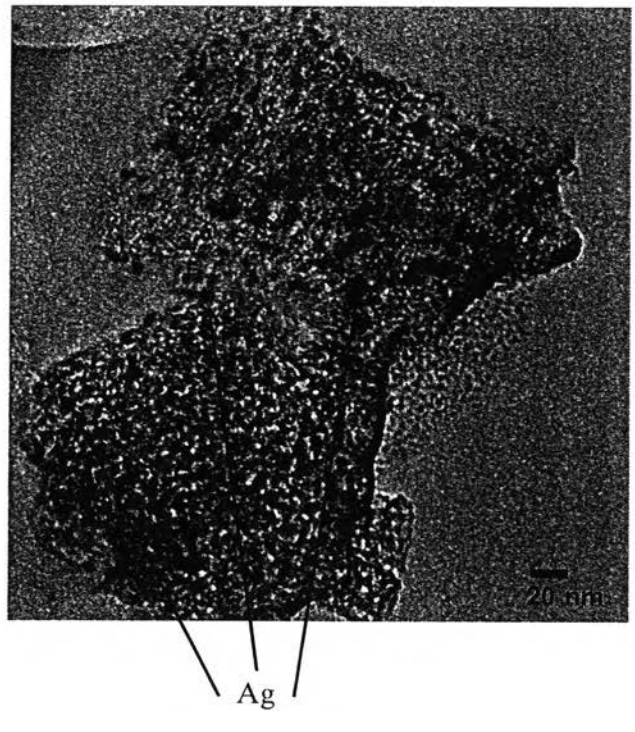

Figure 4.3 TEM images of (a) 13.16 wt.% Ag/Al_2O_3 C, and (b) 14.86 wt.% Ag/α-Al_2O_3.

4.4.1.4 XRD results

The XRD patterns of the $Ag/SrTiO_3$ catalysts with various Ag loadings shown in Figure 4.4 are not much different from that of the pristine support; all of them have highly crystalline structure. The dominant peaks of metallic silver at 2θ of about 28°, 38°, and 44° correspond to (110), (111), and (200) planes, while an extremely small Ag_2O peak was observed at 2θ of 35° [26], indicating that the Ag loaded on the $SrTiO_3$ support was mostly in the metallic form. To compare the crystallite size of all studied catalysts, the most dominant metallic silver peak at 2θ of 38° was used in the calculation. Figure 4.5 compares the crystalline structures of the studied Ag catalysts loaded on different supports at their optimum loadings. The Ag/α-Al_2O_3, $Ag/Al_2O_{3,Acid}$, and Ag/SiO_2 90 catalysts exhibited more X-ray amorphous support structures as compared to the $Ag/SrTiO_3$ catalyst, which showed a highly crystalline support structure. The XRD results also showed that the $Ag/SrTiO_3$ catalyst had the largest Ag crystallite size while the smallest Ag crystallite size was found in the $Ag/Al_2O_{3,Acid}$ catalyst (Table 4.1), which agree well with the particle sizes observed from the TEM images. The XRD and TEM results verify the single crystalline structure of Ag particles in all prepared catalysts, as aforementioned in the SAD pattern result.

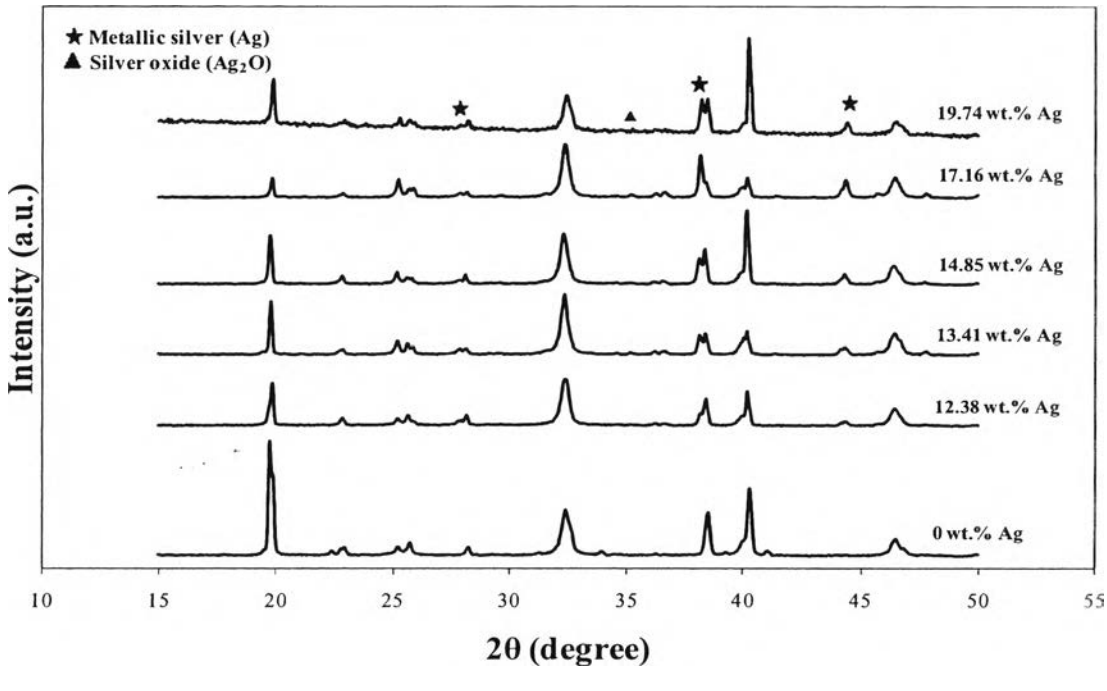

Figure 4.4 XRD patterns of $Ag/SrTiO_3$ catalysts with various Ag loadings.

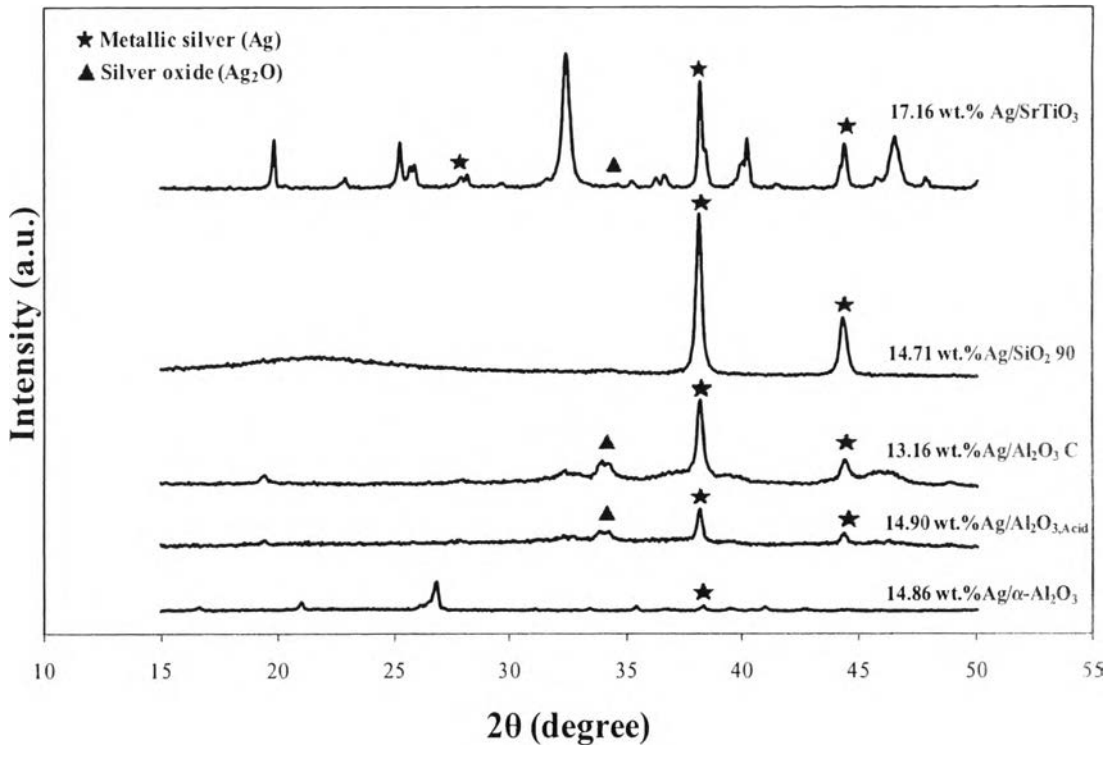

Figure 4.5 XRD patterns of Ag catalysts on different supports at their optimum Ag loadings.

4.4.1.5 TPD profiles of oxygen

Figure 4.6 compares the oxygen TPD profile of the 17.16 wt.% $Ag/SrTiO_3$ catalyst with the TPD profiles of the Ag catalysts on the other supports. The TPD peak at around 600-700 K obtained on the $Ag/Al_2O_{3,Acid}$ catalyst indicates that the $Al_2O_{3,Acid}$ support can provide significant oxygen storage, leading to a better catalytic performance towards ethylene epoxidation as compared to all Al_2O_3 and SiO_2 supported catalysts [7]. There were several broad but extremely small oxygen desorption peaks observed for the Ag/Al_2O_3 C and Ag/SiO_2 90 catalysts, suggesting the low oxygen adsorption capacities of these supports. For the $Ag/SrTiO_3$ catalyst, a much larger oxygen desorption peak was observed at around 620-800 K as compared to that of the $Ag/Al_2O_{3,Acid}$ catalyst. The extremely large desorption peak at 800-1000 K of the $Ag/SrTiO_3$ catalyst results from the decomposition of $SrTiO_3$. The TPD results reveal that the $Ag/SrTiO_3$ catalyst provides a very high oxygen adsorption capacity (Table 4.3) but the high desorption

temperature indicates a stronger bonding energy between oxygen molecules with the $SrTiO_3$ surface as compared to the other Ag catalysts with different supports.

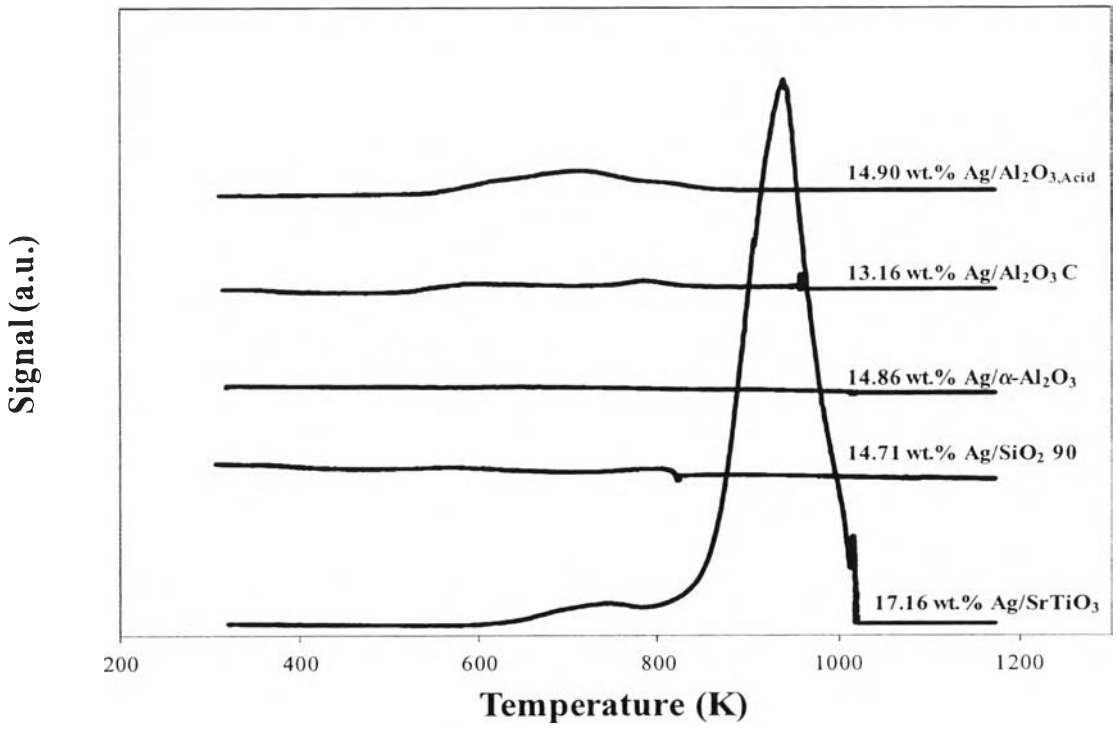

Figure 4.6 TPD profiles of O_2 of studied Ag-loaded catalysts on different supports at their optimum Ag loadings.

4.4.1.6 TPD profiles of ethylene

As shown in Figure 4.7, the $Ag/Al_2O_{3,Acid}$ exhibits a much higher desorption peak of ethylene at 450 K, compared to the other catalysts except the $Ag/SrTiO_3$ catalyst. The O_2 and C_2H_4 uptakes of all studied catalysts are summarized in Table 4.3. The $Ag/SrTiO_3$ catalyst possessed a larger ethylene desorption peak in the temperature range of 600-800 K with a small one at 400-450 K. Again, the extremely large desorption peak of the $Ag/SrTiO_3$ catalyst at 800-1000 K attributes to the decomposition of the $SrTiO_3$ support. Furthermore, the ethylene interaction with the Ag/Al_2O_3 C and Ag/SiO_2 90 catalysts can also be clearly observed by several broad and small peaks, indicating the formation of various compounds at different temperatures. Surprisingly, the Ag/α-Al_2O_3 catalyst showed

the absence of any ethylene desorption peak. Among all of the investigated catalysts, $Ag/SrTiO_3$ exhibited not only the highest O_2 uptake but also the maximum C_2H_4 uptake.

Table 4.3 TPD results of O_2 and C_2H_4 of studied Ag-loaded catalysts on different supports at their optimum Ag loadings (Temperature range of 500-800 K for O_2 and 400-800 K for C_2H_4)

Support	Optimum Ag loading (wt.%)	O_2 uptake (μmol g^{-1})	C_2H_4 uptake (μmol g^{-1})
α-Al_2O_3	14.86	6	0
Al_2O_3 C	13.16	236	185
$Al_2O_{3,Acid}$	14.90	1929	2317
SiO_2 90	14.71	147	103
$SrTiO_3$	17.16	6381	7534
TiO_2	14.67	407	-

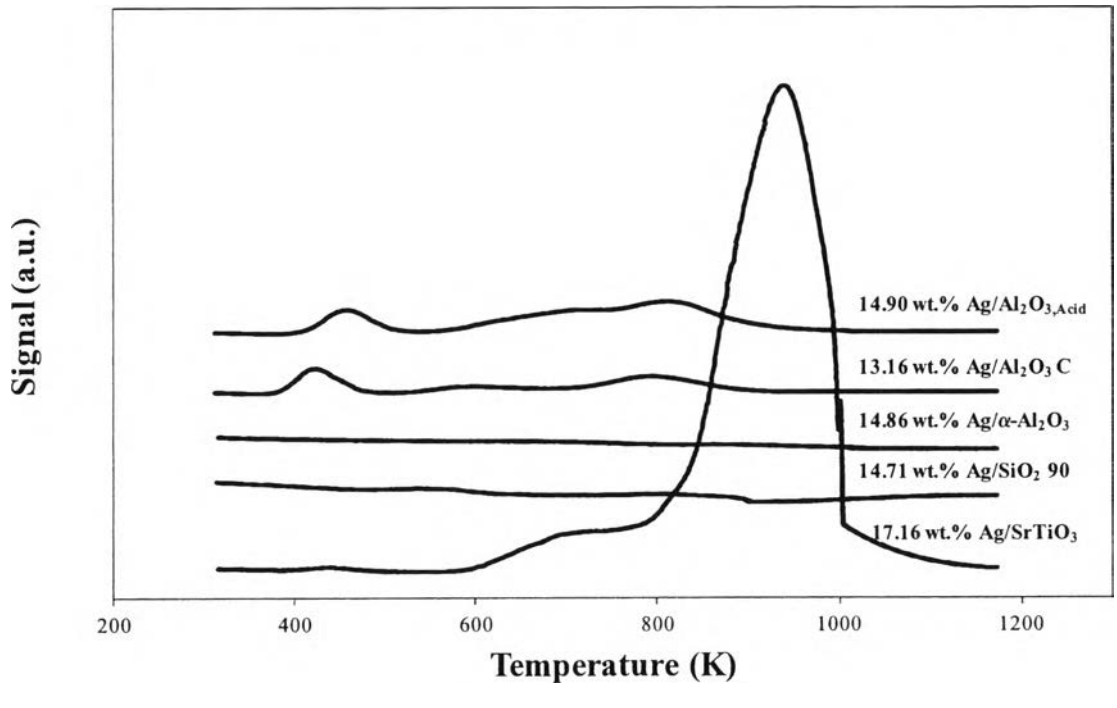

Figure 4.7 TPD profiles of C_2H_4 of studied Ag-loaded catalysts on different supports.

4.4.1.7 XPS results

The deconvoluted Ag 3d XPS peaks of the 17.16 wt.% $Ag/SrTiO_3$ catalyst before and after the reaction are shown in Figure 4.8. The XPS results confirm the presence of both metallic silver (Ag) and silver oxide (Ag_2O) on the catalyst surface both before and after the ethylene epoxidation reaction. The metallic Ag peaks can be clearly seen at the binding energies of 373.5 eV for Ag $3d_{3/2}$ and 367.5 eV for Ag $3d_{5/2}$. On the other hand, the small Ag_2O peaks were observed at the binding energies of 371.5 eV for Ag_2O $3d_{3/2}$ and 366.5 eV for Ag_2O $3d_{5/2}$ [25]. Prior to the reaction, the ratio of Ag to Ag_2O was about 11.5, and it decreased to 4.5 after the reaction. This indicates that some metallic Ag was oxidized to form Ag_2O during the reaction.

(a) (b)

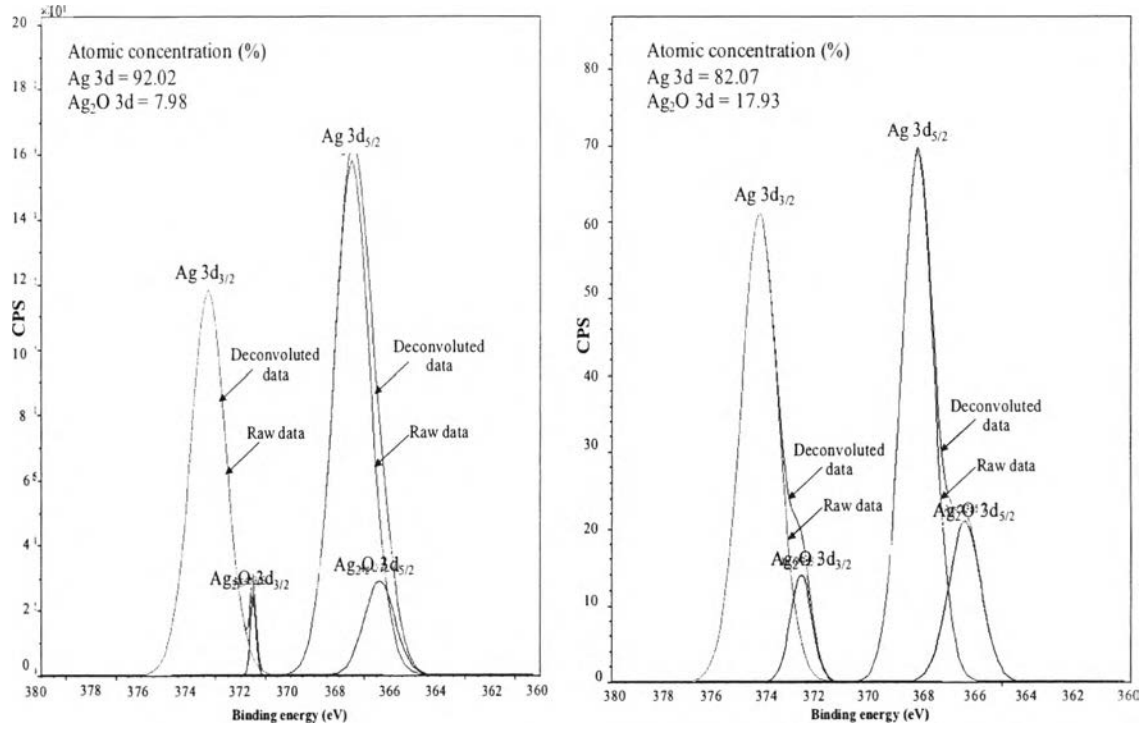

Figure 4.8 Deconvoluted Ag 3d XPS peaks of 17.16 wt.% $Ag/SrTiO_3$ catalyst: (a) before the reaction and (b) after the reaction.

4.4.2 Ethylene epoxidation activity results

The effect of reaction temperature on the ethylene epoxidation activity and selectivity over the Ag catalysts on different supports (α-Al_2O_3, Al_2O_3 C, $Al_2O_{3,Acid}$, SiO_2 90, $SrTiO_3$ and TiO_2) at their optimum Ag loadings is summarized in Table 4.2. Table 4.2 shows that the C_2H_4 conversion increases as the reaction temperature increases from 498 to 563 K. In contrast, the EO selectivity decreased with increasing reaction temperature from 498 to 563 K, except for the Ag/$SrTiO_3$ catalyst, where the selectivity still remained very high. For any given studied catalysts, the EO yield increased up to a certain temperature. After that, the yield considerably decreased with further increasing reaction temperature. This is because a higher temperature simply promotes complete oxidation, as confirmed experimentally by the increase in CO_2 [7,27]. Among the studied catalysts, the 17.16 wt.% Ag/$SrTiO_3$ was found to be the best catalyst, providing both the highest EO yield of 4.5 % with the maximum EO selectivity up to 99 %. Interestingly, this catalyst produced no CO_2 at reaction temperatures below 548 K. These results can be well related to the TPD results of O_2 and C_2H_4 of this catalyst (Figures 4.6 and 4.7), which showed the high adsorption capabilities of O_2 and C_2H_4 (Table 4.3). The high desorption temperatures of both oxygen and ethylene on the surface of the Ag/$SrTiO_3$ catalyst favor the epoxidation reaction over the complete oxidation at low temperatures (less than 548 K) [28]. The Ag/$SrTiO_3$ catalyst also had the largest Ag particle size with low Ag dispersion. It was found that the larger the Ag particle size, the lower the opportunity of secondary reactions including complete oxidation, leading to increasing EO yield [29,30]. However, when the Ag particle size further increased by increasing Ag loading to greater than 17.16 wt.%, a significant decrease in the catalytic activity was observed. These results imply that Ag particle sizes that are too high or too low are detrimental for the epoxidation reaction performance.

Table 4.2 Ethylene epoxidation activity of selected Ag-loaded catalysts at different reaction temperatures (6% O_2 and 6% C_2H_4 balanced with He, a space velocity of 6000 h^{-1}, a pressure of 24.7 psia)

Support	Optimum Ag loading (wt.%)	Reaction Temperature (K)	C_2H_4 conversion (%)	EO selectivity (%)	EO yield (%)
α-Al_2O_3	14.86	498	1.7	98.1	1.7
		523	2.7	87.5	2.3
		548	3.6	77.4	2.8
		563	4.6	38.5	1.8
Al_2O_3 C	13.16	498	0.8	96.5	0.8
		523	1.4	89.9	1.2
		548	3.9	86.7	3.4
		563	4.9	27.0	1.3
$Al_2O_{3,Acid}$	14.90	498	2.1	99.2	2.1
		523	3.3	96.4	3.2
		548	4.0	64.9	2.6
		563	4.5	48.2	2.2
		573	5.1	19.2	1.0
SiO_2 90	14.71	498	1.9	84.3	1.6
		523	3.6	82.1	3.0
		548	4.4	86.4	3.8
		563	5.0	17.3	0.9
$SrTiO_3$	17.16	498	0.9	97.4	0.9
		523	2.3	97.7	2.2
		548	4.6	99.0	4.5
		563	4.8	51.1	2.5
TiO_2	14.67	498	1.0	76.8	0.8
		523	1.3	72.9	0.9
		548	2.5	69.7	1.8
		563	3.0	10.2	0.3

The $Ag/Al_2O_{3,Acid}$ catalyst gave a comparable EO yield to the $Ag/SrTiO_3$ catalyst, but with a relatively high EO selectivity at the reaction temperature below 523 K, probably resulting from an appropriate acidic property that might help suppress the formation of CO_2 [31]. This catalyst possessed the smallest Ag particle size and moderate Ag dispersion with the relatively high O_2 and C_2H_4 uptakes (Table 4.3). These results indicate that the ethylene epoxidation reaction depends not only the reaction temperature, Ag loading, and specific surface area, but also the Ag particle size, Ag dispersion on the supports and finally the bonding energy of both O_2 and C_2H_4 with the surface of catalyst support. The optimum conditions for ethylene epoxidation were found to correspond to large Ag particle sizes of about 50 nm, low specific surface area, low Ag dispersion, appropriate amount of Ag loading and the strong bonding of both O_2 and C_2H_4 with the $SrTiO_3$ support, as evidenced from the best activity results of the 17.16 wt.% $Ag/SrTiO_3$ catalyst. It can also be concluded that moderate Ag particle sizes favor the high yield of EO and that the Ag dispersion clearly affects the EO selectivity [17]. For instance, the Ag/SiO_2 90 catalyst with high Ag dispersion gave low EO selectivity because the relatively small Ag particles dispersed on the support easily interacted with the reactants and formed CO_2 through secondary reactions.

Figure 4.9 compares the catalytic performance of the Ag/TiO_2 catalyst (which represented a TiO_2 support prepared by a sol-gel process) with the $Ag/SrTiO_3$ catalyst (which was found to be the best catalyst, as aforementioned). The $Ag/SrTiO_3$ catalysts with various Ag loadings were found to exhibit a much better catalytic activity towards the ethylene epoxidation reaction, providing both the enhancement of EO yield up to 4.5 % and EO selectivity up to 99 % at the Ag loading of 17.16 wt.%. This result implies that the nature of the support plays the dominant role in making a catalyst more selective. The EO yield and EO selectivity dropped at a very high Ag loading greater than 15 wt.% for the Ag/TiO_2 catalyst. Again, it should be remarked that the Sr atoms that are incorporated in the $SrTiO_3$ support clearly affect in the superior performance of $Ag/SrTiO_3$ catalyst.

(a)

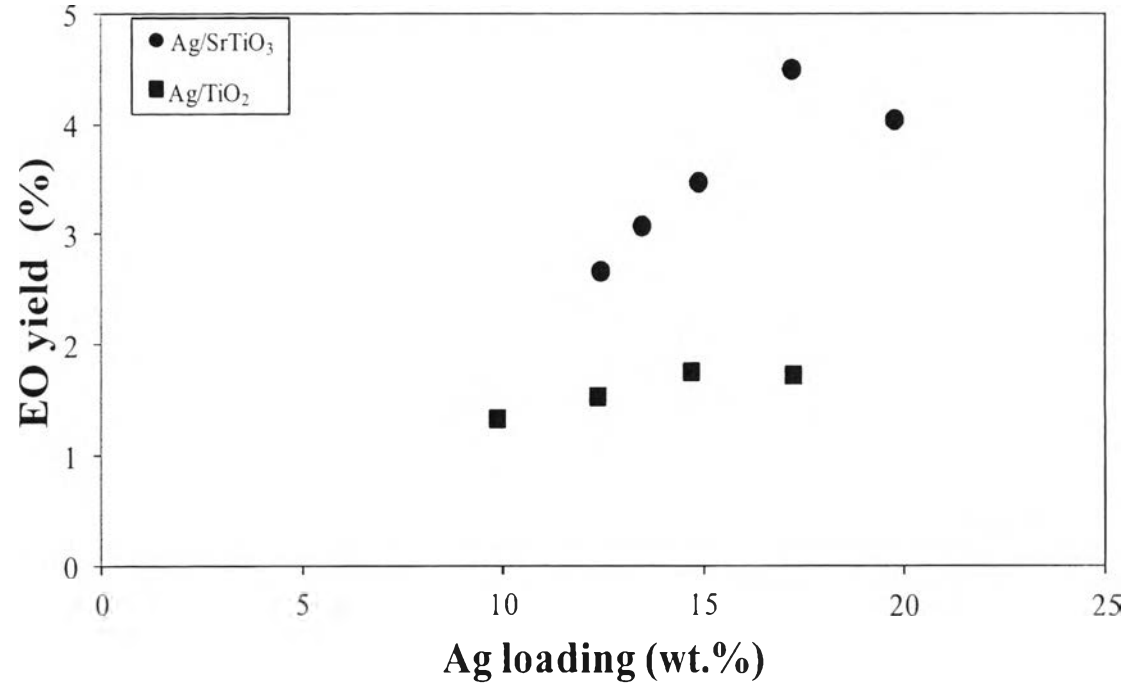

(b)

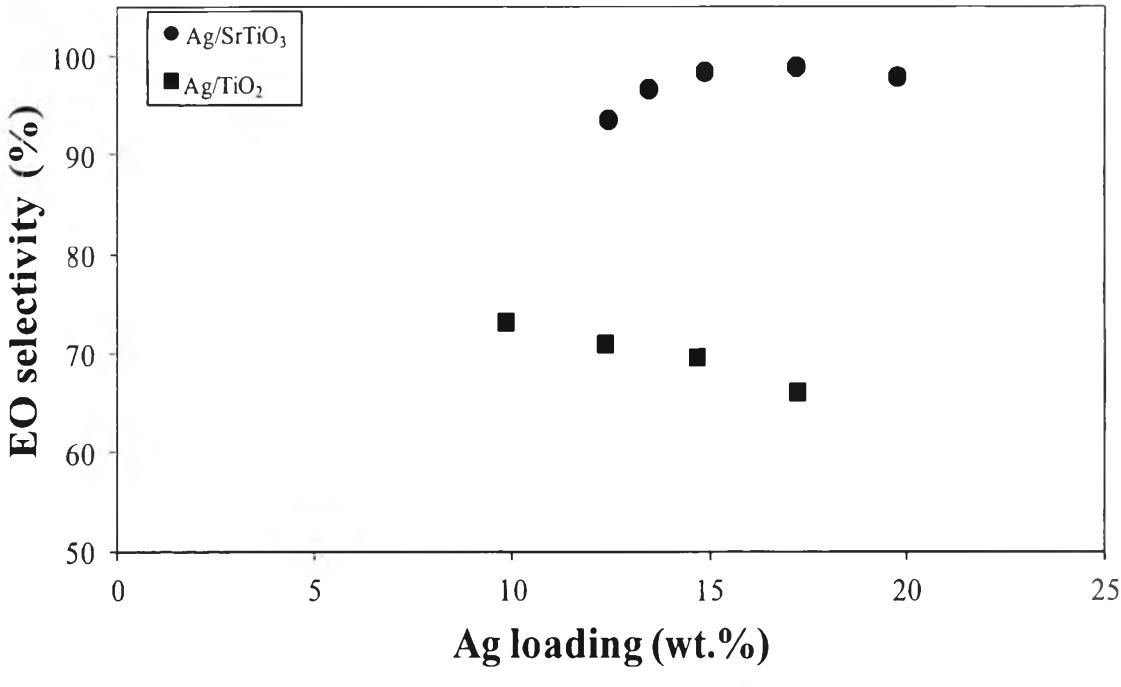

Figure 4.9 EO yield (a) and EO selectivity (b) as a function of Ag loading on $SrTiO_3$ and TiO_2 supports (6% O_2 and 6% C_2H_4 balanced with He, a space velocity of 6000 h^{-1}, a pressure of 24.7 psia, a temperature of 548 K).

After the reaction experiments, the spent 17.16 wt.% $Ag/SrTiO_3$ catalyst was also characterized by XRD, TEM, XPS, and TG-DTA. The XRD patterns of this catalyst before and after the reaction were almost the same, indicating no significant change in the crystalline structure. The average Ag particle sizes obtained from the TEM images slightly increased from 58.64 nm for the fresh catalyst to 61.73 nm for the spent catalyst, implying a very small extent of sintering of the catalyst during the epoxidation reaction. As previously mentioned for the XPS results (Figure 4.8), a significant amount of the metallic silver phase was changed to Ag_2O phase after the reaction. In addition, the coke formation on all the spent catalysts from the TG-DTA analysis is comparatively shown in Table 4.4. The $Ag/SrTiO_3$ catalyst had coke formation of 6.84 %, similar to the Ag/α-Al_2O_3 and Ag/TiO_2 catalysts but lower than the Ag/SiO_2 90 catalyst. These results imply that the higher Ag dispersion of the Ag/SiO_2 90 catalyst (Table 1) can lead to more coke formation.

Table 4.4 Coke formation on spent Ag-loaded catalysts after the ethylene epoxidation reaction (6% O_2 and 6% C_2H_4 balanced with He, a space velocity of 6000 h^{-1}, a pressure of 24.7 psia)

Support	Optimum Ag loading (wt.%)	Optimum reaction temperature from Table 2 (K)	Coke formation (%)
α-Al_2O_3	14.86	548	4.3
Al_2O_3 C	13.16	548	2.3
$Al_2O_{3,Acid}$	14.90	523	1.7
SiO_2 90	14.71	548	10.9
$SrTiO_3$	17.16	548	6.8
TiO_2	14.67	548	6.7

The stability in terms of EO yield and EO selectivity as a function of time on stream of the 17.16 wt.% $Ag/SrTiO_3$ catalyst (the optimum catalyst) was also investigated, as shown in Figure 4.10. It should be noted that the catalytic performance of all investigated catalysts was compared at 6 h of time on stream. The EO selectivity slightly dropped from 99 % at 6 h to 84 % after 32 h of experiment and remained almost stable at this level. The coke formation is believed to cause the reduction of both EO selectivity and yield. The yield of EO also depicted the same trend, decreasing from 4.5 % to 3.3 % after 32 h. It can be concluded that this catalyst not only producing the maximum EO yield and EO selectivity but also providing a long-term stability of the catalytic performance. A slight increase of the oxygen ratio in feed may be needed to reduce the coke formation and the use of a larger amount of catalyst is recommended to obtain a high ethylene conversion as found in the industrial process.

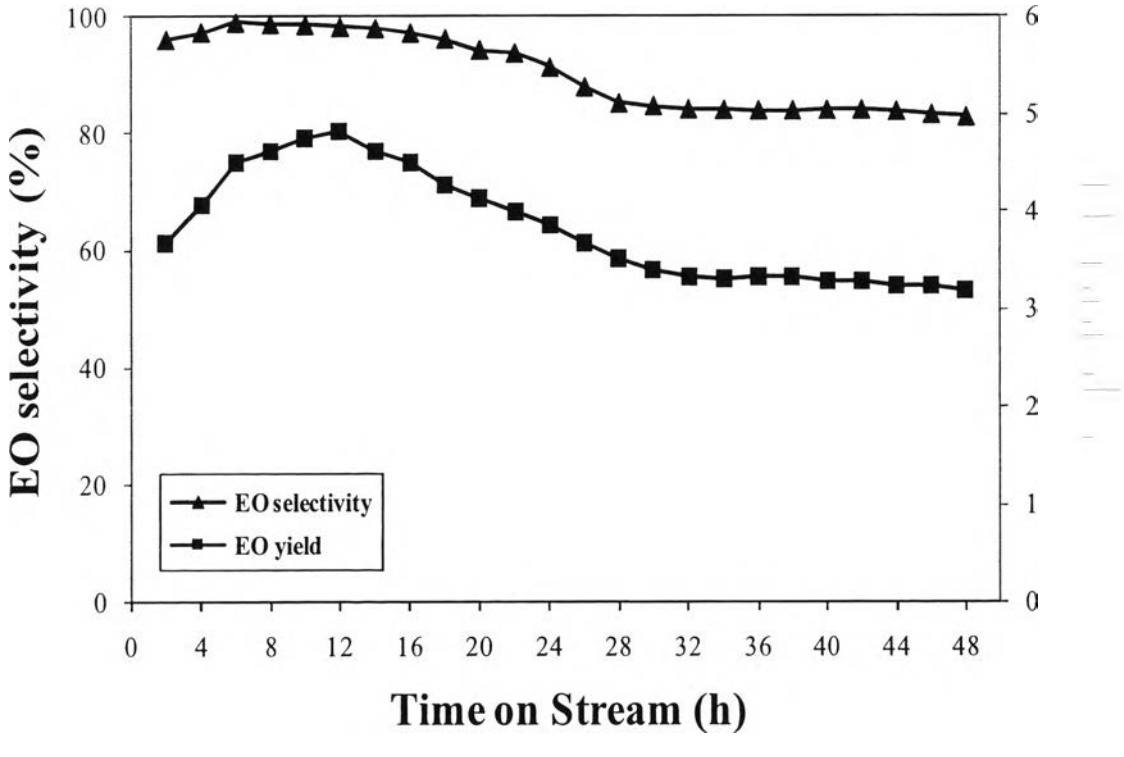

Figure 4.10 EO selectivity and EO yield as a function of time on stream for 17.16 wt.% $Ag/SrTiO_3$ catalyst (6% O_2 and 6% C_2H_4 balanced with He, a space velocity of 6000 h^{-1}, a pressure of 24.7 psia, a temperature of 548 K).

4.5 Conclusions

In this study, Ag supported on $SrTiO_3$ was proved to be an effective catalyst for epoxidation of ethylene, giving unusually high selectivities and yields of ethylene oxide, compared to Ag catalysts supported on other oxide supports ($Al_2O_{3,Acid}$, Al_2O_3 C, α-Al_2O_3, SiO_2 90 and TiO_2). The most promising catalyst for EO production was found to be the 17.16 wt.% $Ag/SrTiO_3$, which provided the highest EO yield of 4.5 % with the EO selectivity up to 99 % at the reaction temperature of 548 K. Moreover, the $Ag/SrTiO_3$ catalyst produced no CO_2 at the reaction temperature below 548 K. The performance of the $Ag/SrTiO_3$ catalyst may be related to its high oxygen and ethylene adsorption ability (high uptakes of both ethylene and oxygen) as well as moderate size of Ag particles compared to the other catalysts investigated. Moreover, Sr atoms that are incorporated in the $SrTiO_3$ support play an important role in making this catalyst more selective in EO formation. The effects of Sr atoms that are incorporated in the $SrTiO_3$ support on the catalytic performance and mechanism will be described in details in our next manuscript.

4.6 Acknowledgements

This work was supported by The Royal Golden Jubilee Ph.D. Program (RGJ-Industry) awarded by Thailand Research Fund with the in-kind support from PTT Global Chemical Public Co. Ltd.; the Sustainable Petroleum and Petrochemicals Research Unit, Center of Excellence on Petrochemical and Materials Technology, Chulalongkorn University (Thailand); and the Transportation Energy Center, Department of Chemical Engineering, University of Michigan (USA).

4.7 References

[1] J.T. Jankowiak, M.A. Barteau, J. Catal. 236 (2005) 379-386.

[2] Y.Ch. Kim, N.C. Park, J.S. Shin, S.R. Lee, Y.J. Lee, D.J. Moon, Catal. Today 87 (2003) 153-162.

[3] J. Lacson, Ethylene Oxide, in: Chemical Economics Handbook, Menlo Park, CA: SRI International, 2003.

[4] G. Ertl, H. Knozinger, J. Weitkamp, Handbook of Heterogeneous Catalysis, VCH, Weinheim, 1997.

[5] Y.S. Yong, E.M. Kennedy, N.W. Cant, Appl. Catal. 76 (1991) 31-39.

[6] S. Matar, M.J. Mirbach, H.A. Tayim, Catalysis in Petrochemical Processes, Kluwer Academic Publishers, The Netherlands, 1989, pp. 85.

[7] S. Rojluechai, Ph.D. Dissertation, The Petroleum and Petrochemical College, Chulalongkorn University, Bangkok, Thailand, 2006.

[8] S. Rojluechai, S. Chavadej, J.W. Schwank, V. Meeyoo, Catal. Commun. 8 (2007) 57-64.

[9] P. Harriott, J. Catal. 21 (1971) 56-64.

[10] J.S. Beck, J.C. Vartuli, W.J. Roth, M.E. Leonowicz, C.T. Kresge, K.D. Schmitt, C.T.W. Chu, D.H. Olson, E.W. Sheppard, S.B. McCullen, J.B. Higgins, J.L. Schlenker, J. Am. Chem. Soc. 114 (1992) 1-11.

[11] A.P. Fotopoulos, K.S. Triantafyllidis, Catal. Today 127 (2007) 148-156.

[12] T. Puangpetch, T. Sreethawong, S. Yoshikawa, S. Chavadej, J. Mol. Catal. A: Chem. 287 (2008) 70-79.

[13] A. Ayame, Y. Uchida, H. Ono, M. Miyamoto, T. Sato, H. Hayasaka, Appl. Catal. A: Gen. 244 (2003) 59-70.

[14] G.B. Hoflund, D.M. Minahan, Nucl. Instrum. Meth. B 118 (1996) 517-521.

[15] S. Linic, M.A. Barteau, J. Am. Chem. Soc. 125 (2003) 4034-4035.

[16] J.G. Serafin, J. Mol. Catal. A: Chem. 131 (1998) 157-168.

[17] S.S. Hassani, M.R. Ghasemi, M. Rashidzadeh, Z. Sobat, Cryst. Res. Cryst. Technol. 44 (2009) 948-952.

[18] P. Christopher, S. Linic, Chem. Cat. Chem. 2 (2010) 78-83.

[19] T. Puangpetch, T. Sreethawong, S. Yoshikawa, S. Chavadej, J. Mol. Catal. A: Chem. 312 (2009) 97-106.

[20] T. Puangpetch, T. Sreethawong, S. Chavadej, Int. J. Hydrogen Energ. 35 (2010) 6531-6540.

[21] T. Puangpetch, P. Sommakettarin, S. Chavadej, T. Sreethawong, Int. J. Hydrogen Energ. 35 (2010) 12428-12442.

[22] T. Puangpetch, S. Chavadej, T. Sreethawong, Energ. Convers. Manage. 52 (2011) 2256-2261.

[23] B.D. Cullity, Elements of X-ray Diffraction, Addison-Wesley Pub. Co., MA, 1978.

[24] A.G. Jackson, Handbook of Crystallography, Springer-Verlag, New York, 1991.

[25] J.F. Moulder, W.F. Stickle, P.E. Sobol, K.D. Bomben, Handbook of X Ray Photoelectron Spectroscopy: A Reference Book of Standard Spectra for Identification and Interpretation of XPS Data, Physical Electronics, 1995.

[26] J.V. Smith, X-Ray Powder Data File, American Society for Testing Materials, PA, 1960.

[27] M.O. Ozbek, I. Onal, R.A. Santen, ChemCatChem. 3 (2011) 150-153.

[28] R.A. Santen, H.P.C.E. Kuipers, Adv. Catal. 35 (1987) 265-321.

[29] J. Lu, J.J. Bravo, A. Takahashi, M. Haruta, S.T. Oyama, J. Catal. 232 (2005) 85-95.

[30] F. Zemicheael, A. Palermo, M. Tikhov, R. Lambert, Catal. Lett. 80 (2002) 93.

[31] Z. Gao, Y. Shi, J. Nat. Gas Chem. 19 (2010) 173-178.